Semiconductor core-level to valence-band maximum binding-energy differences: Precise determination by x-ray photoelectron spectroscopy

E. A. Kraut, R. W. Grant, J. R. Waldrop, and S. P. Kowalczyk
Microelectronics Research and Development Center, Rockwell International, Thousand Oaks, California 91360
(Received 10 December 1982)

Angle-resolved core-level and valence-band x-ray photoelectron spectroscopy (XPS) data for GaAs(110), Ge(110), and Ge(111) surfaces are analyzed to determine core-level to valence-band maximum binding-energy differences to a precision of the order of the room-temperature thermal energy. A method for markedly improving the precision with which the position of the valence-band maximum in XPS data can be located is presented. This method is based on modeling the XPS valence-band spectrum in the vicinity of the valence-band maximum by an instrumentally broadened theoretical valence-band density of states and fitting this model to the experimental data by using the least-squares method. The factors which influence the attainable precision for determining core-level to valence-band maximum binding-energy differences are quantitatively discussed. These factors include the presence of occupied surface states, band bending, surface chemical shifts, background effects associated with inelastic processes, instrumental line shape, and spectrometer calibration accuracy. The spin-orbit—split components of the Ga, As, and Ge $3d$ core lines are resolved and binding energies of these components, measured relative to the valence-band maxima in GaAs and Ge, are reported.

I. INTRODUCTION

X-ray photoelectron spectroscopy (XPS) is well known for its usefulness in detecting the presence of specific elements by means of binding-energy measurements and for its ability to follow chemical-compound formation through observation of changes in binding energy (chemical shifts) and changes in photoelectron line shape.[1] A less frequently exploited use of XPS is to monitor the potential at a semiconductor interface.[2] In this way it becomes possible to make accurate determinations of band bending, Schottky-barrier heights, and heterojunction band discontinuities.[3] Accurate XPS determination of the above quantities requires that experimental values of core-level to valence-band maximum binding-energy differences be known with a precision on the order of plus or minus the room-temperature thermal energy (0.025 eV). Recently we reported on a method of achieving this level of precision.[3] The purpose of the present paper is to provide further important details, and to report new results for the binding energies of the spin-orbit—split components of the $3d$ core lines in Ge and GaAs measured relative to the valence-band maximum (E_v).

The application of XPS (and other photoelectron spectroscopies) to monitor semiconductor interface potentials depends on locating E_v relative to the Fermi level E_F at the interface. This application is illustrated in Fig. 1 for a vacuum-semiconductor interface. Near the interface the local charge-density distribution may differ from that deeper in the bulk semiconductor. Consequently, Poisson's equation predicts a spatially varying electrostatic potential which bends all of the bands or energy levels by an amount that depends only on the distance from the interface. This assumes that the energy band gap in the space-charge region is the same as it is deeper in the bulk semiconductor. For semiconductor x in Fig. 1, the energy of a core-level E^x_{CL}, the valence-band maximum E^x_v, and the conduction-band minimum E^x_c are shown in the bulk (b) and at an interface (i). Binding energy E_B is measured with respect to $E_F(E_B=0)$. The band gap E^x_g, position of the Fermi level in the bulk relative to E^x_v,δ^x, band-bending potential V^x_{BB}, and depletion layer width W are also shown in Fig. 1.

It follows from Fig. 1 that the band-bending potential V^x_{BB} at the interface is given by

$$qV^x_{BB}=(E^x_{\mathrm{CL}}-E^x_v)+\delta^x-E^x_{\mathrm{CL}}(i)\,, \tag{1}$$

where q is the electronic charge. The core-level to valence-band-edge binding-energy difference $E^x_{\mathrm{CL}}-E^x_v$ and

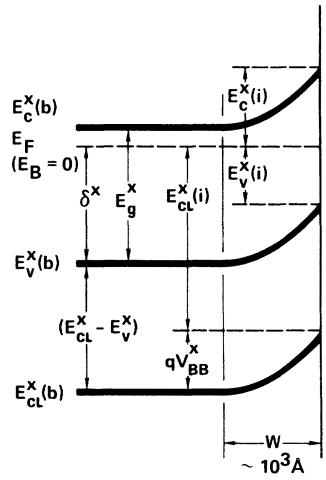

FIG. 1. Generalized energy-band diagram at an abrupt semiconductor-vacuum interface.

 ©1983 The American Physical Society

δ^x are material properties of semiconductor x. The photoelectron potential monitoring method consists of determining the band-bending potential V_{BB}^x from Eq. (1) by measuring $E_{\rm CL}^x(i)$, given knowledge of the material parameters $E_{\rm CL}^x - E_v^x$ and δ^x.

Core-level to valence-band maximum binding-energy differences can be measured by several photoelectron spectroscopies. Each technique has its own advantages and limitations. The presently available energy resolution of XPS may not be as good as some other photoelectron spectroscopies which utilize lower kinetic energy photoelectrons. However, the greater photoelectron escape depth typically associated with XPS measurements averages the photoelectron signal over many atom layers, which can be an advantage for minimizing complexities due to interface—chemical-shift and interface-potential variations. This paper focuses on optimizing the XPS technique for high-precision $E_{\rm CL}^x - E_v^x$ measurements.

In this paper we report binding energies of the $3d$ electrons in GaAs and Ge measured relative to E_v^x. For a semiconductor x of the zinc-blende type (e.g., GaAs), a schematic relation between the XPS spectrum, density of states, and energy bands is shown in Figs. 2(a)—2(c), respectively. Several previous measurements of the $3d$ binding energies in GaAs and Ge have been reported.[4–7] In general, the precision of the previous measurements has been limited to about ± 0.1 eV. In this paper we shall examine, in detail, factors which affect the determination of $E_{\rm CL}^x - E_v^x$ and of the spin-orbit—split components $E_{3d_{3/2}}^x - E_v^x$ and $E_{3d_{5/2}}^x - E_v^x$ shown in Fig. 2(a) to a precision on the order of the room-temperature thermal energy. The experimental procedure and results for GaAs and Ge are presented in Sec. II. Data analysis is discussed in Sec. III, and the paper is summarized in Sec. IV.

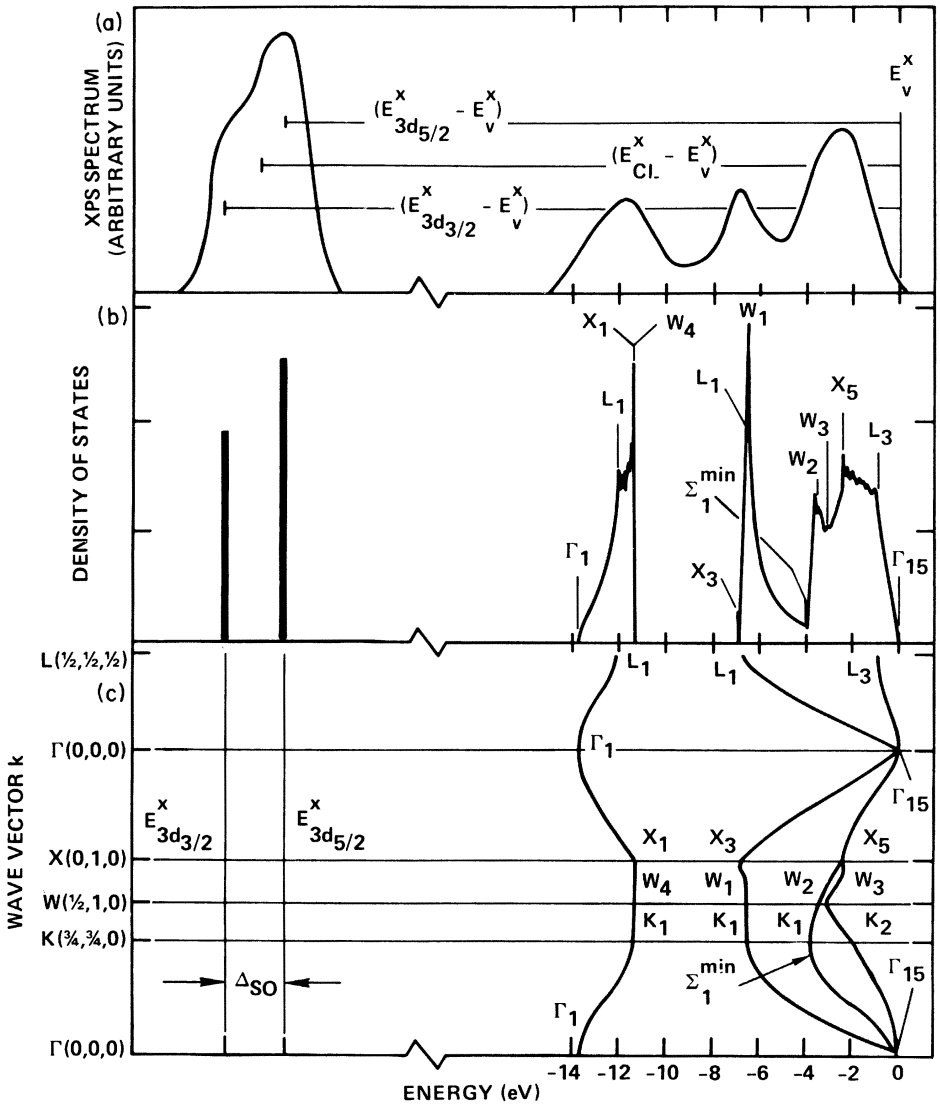

FIG. 2. (a) Schematic XPS core- and valence-band spectrum showing the valence-band edge E_v^x, the center $E_{\rm CL}^x$ of a $3d$ core level and its spin-orbit—split components $E_{3d_{3/2}}^x$ and $E_{3d_{5/2}}^x$. (b) Schematic zinc-blende valence-band density of states (VB DOS) and δ-function spin-orbit—split $3d$ core-level components. (c) Schematic zinc-blende valence-band structure and dispersionless spin-orbit—split (Δ_{so}) $3d$ core-level components.

II. EXPERIMENTAL

To obtain high-precision $E^x_{CL}-E^x_v$ measurements, it was necessary to consider several experimental details. The important aspects of the experimental procedure and the experimental results are discussed in this section.

A. Spectrometer description

The electron spectrometer utilized for XPS measurements in this study was an ultrahigh-vacuum (UHV) modified Hewlett-Packard model 5950A, which employs a monochromatized Al$K\alpha$ ($h\nu=1486.6$ eV) x-ray source. The average photoelectron kinetic energy excited from the GaAs and Ge valence bands and from the 3d core levels of Ga, Ge, and As corresponds to an escape depth of ~ 27 Å.[8] The photoelectron-emission direction relative to the sample normal was kept fixed at 51.5° for all measurements so that the effective photoelectron escape depth was ~ 17 Å; thus the photoelectron signal was averaged over many atomic planes near the sample surface.

The bakable sample preparation chamber was equipped with a low-energy electron-diffraction (LEED) system and a rastered ion-sputter gun. Both ion pumps and cryopumps were used to achieve a base pressure of $\approx 1\times 10^{-10}$ Torr. Titanium sublimation pumping was also employed to minimize reactive background gases. The sample holder had a heater and thermocouple arrangement, which was used to control the annealing temperatures of samples. All XPS measurements reported here were taken at or near room temperature.

The XPS spectrometer was equipped with a low-energy electron flood gun. Core-level spectra were taken with and without low-energy (~ 5 eV) electron illumination to test for sample charging due to x-ray illumination. No charging effects were observed for the samples used in this study.

The analyzer of the XPS spectrometer used in this work had a half-angle acceptance cone of $\sim 2°$ so that data obtained with this instrument are angle resolved. This angular-resolution capability was utilized to test if the measured photoelectron spectrum in the vicinity of the valence-band maximum was affected by occupied surface-state contributions (see Sec. III A 2).

B. Spectrometer calibration

A key factor required to perform highly accurate XPS measurements is the precise calibration of the binding-energy scale. All XPS data reported herein were obtained by repeatedly scanning a 50-eV binding-energy interval until the desired statistical accuracy was obtained. To calibrate this 50-eV binding-energy interval, a precise measurement of the retarding voltage on the HP5950A XPS spectrometer electron-optics lens system was made. A high-impedance voltage-divider network was used for this measurement. The retarding lens voltage was first reduced by a precision 1000:1 voltage divider, and was then compared against a seven-place voltage calibrator with a sensitive null meter. The apparent binding energy of the Au $4f_{7/2}$ photoelectron peak from an Au calibration sample was monitored as a function of retarding lens voltage. By making several measurements of the Au $4f_{7/2}$ photoelectron peak position as a function of the retarding lens voltage, it was found that the binding-energy scale could be routinely calibrated to 0.02%. No systematic ramp-voltage linearity deviation could be detected at this level of precision. The collection of valence-band spectra required long (typically ~ 12 h) counting times to obtain the desired statistical accuracy. The spectrometer energy scale was calibrated before and after these experiments to be sure that calibration variations larger than 0.02% were not present.

C. Sample selection and preparation

The single-crystal GaAs and Ge samples used in this study were oriented wafers cut from bulk-grown material. The GaAs wafers had (110) orientation, while both (111)- and (110)-oriented Ge wafers were studied. Laue back-reflection x-ray photography was used to confirm that the wafers were within 1° of the desired orientation. The orientation of low-index crystallographic axes was also determined, and it was possible to mount samples in the XPS spectrometer with a known angular orientation relative to the photoelectron emission direction of $\leq 2°$.

As mentioned previously, the substantial escape depth of x-ray-excited outer core-level photoelectrons averages the photoelectron signal over many atom layers. For this reason it is desirable to use modestly or lightly doped semiconductors for study to avoid complications due to band bending within the photoelectron escape depth. The typical band-bending length for a 10^{17}-cm^{-3}—doped semiconductor is $\sim 10^3$ Å. As shown in Sec. III D 1, this band bending will not substantially affect the accuracy of the XPS ($E^x_{CL}-E^x_v$) determination. Thus $\sim 10^{17}$-cm^{-3} doping represents a convenient doping-density upper limit in order to avoid XPS measurement complications of band bending. The GaAs samples used in this study were n type, $\sim 5\times 10^{16}$ cm^{-3}; the Ge samples were undoped (slightly n type). It is, of course, desirable to select samples which have relatively low resistivity in order to avoid sample charging during the XPS measurements; for some semiconductors, this could set a useful lower limit on doping density.

Both the GaAs and Ge samples were chemically etched a few minutes prior to insertion into the XPS spectrometer. The GaAs etch was freshly prepared 4:1:1 (H_2SO_4:H_2O_2:H_2O); the Ge etch was dilute HF. The samples were quenched in H_2O and blown dry with N_2. They were then attached to Mo-sample platens with In, which required heating in air to ≈ 160 °C. After a bakeout procedure to achieve UHV, atomically clean and ordered surfaces were prepared by repeated sputtering and annealing cycles. The sputtering gas was Ar, and Ti sublimation pumping was used during sputtering to minimize reactive gases. The GaAs samples were sputtered with ion energies of ~ 600 eV and annealed at ~ 575 °C; Ge samples were sputtered at ~ 2 keV and annealed at ~ 600 °C. LEED measurements determined the surface ordering and removal of sputter damage. The GaAs(110) surfaces exhibited characteristic 1×1 patterns, while the Ge(111) surfaces had 2×8 patterns. The LEED pattern for the Ge(110) surfaces was complex and resembled the reported[9,10] $c(8\times 10)$ pattern characteristic of room-temperature Ge (110). XPS measurements before and after data collection

were used to determine the absence of detectable (≤ 0.1 monolayer) oxygen or carbon contamination.

D. XPS measurements

To minimize experimental difficulties associated with variations in apparent binding energies caused by spectrometer power-supply instabilities and sample position variations, the XPS data were collected by repeatedly scanning (~ 500 scans) a 50-eV binding-energy interval which contained both the core level of interest and the valence-band region until the desired statistical accuracy was obtained. The valence-band and core-level data were thus collected simultaneously from precisely the same spot (an area of ~ 3 mm^2) on the sample. The ramp-voltage scan rate was 1 eV/s. This scan rate was found to be convenient in that it was slow enough to average out high-frequency power-supply noise, and yet fast enough to average out long-term power-supply voltage drifts. By always collecting the core-level and valence-band data simultaneously, instabilities in the spectrometer tended to have an equivalent effect on the apparent core-level and valence-band binding energies. Thus it was possible to always make energy-difference measurements rather than independent absolute determinations.

Several experiments were carried out to examine the reliability of this approach. The binding-energy difference between the Ga $3d$ and As $3d$ core levels was measured several times for GaAs(110) samples with various electron-emission directions. It was observed that the variation of the binding energy of a core level was less than ± 0.1 eV due to sample position variations, surface band-bending variations, spectrometer instability, etc.; the binding-energy difference between the two core levels was reproducible to better than ± 0.01 eV. In previous studies[11,12] of Ge-GaAs heterojunctions, by using an identical measurement technique, it was also found from several measurements on the same sample that outer core-level binding-energy differences could be measured with a reproducibility of less than 0.01 eV and usually less than 0.005 eV.

A primary difficulty with the determination of E_v^x in XPS spectra is a minimization of valence-band spectral distortion due to occupied surface states in the vicinity of E_v^x. Our approach (see Sec. III A 2 for details) is to analyze and compare results for several sets of angle-resolved measurements. Because the XPS photoelectron cross section should depend on the orbital character of filled surface states,[13,14] it should be possible to detect the presence or absence of these states by studying the angular variation of the XPS valence-band spectrum in the vicinity of E_v^x. In Fig. 3 a convenient polar-coordinate system is defined to relate the photoelectron emission direction $\vec{e}$ to crystallographic axes for (110) and (111) surfaces. The polar angle θ for all measurements was held at 51.5°, and only the aximuthal angle ϕ was varied.

1. GaAs

Six sets of angle-resolved XPS data were collected on (110)-oriented GaAs samples. The (110) plane was chosen for study as it is the cleavage plane, and considerable information regarding the surface geometry exists.[15,16] It has been demonstrated that no detectable difference exists in the 1×1 LEED patterns for cleaved and sputter-annealed surfaces.[17] The surface chemical shifts for the Ga $3d$ and As $3d$ photoelectron lines have been measured.[18] Detailed analyses of the surface electronic structures have been carried out.[19–21] The orbital character of the GaAs(110) surface states has been considered in detail.[19] To assess the effect of surface-state contributions on the Ga $3d$ and As $3d$ to E_v^{GaAs} binding-energy difference measurements (see the analysis in Sec. III A 2), XPS data were collected for $\phi = 0°$, 35°, and 90°.

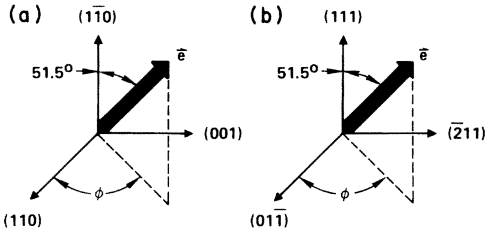

FIG. 3. Polar-coordinate systems relating photoelectron-emission direction $\vec{e}$ to crystallographic axes for (110) and (111) crystal surfaces (left and right, respectively). The azimuthal angle ϕ is in the plane of the crystal surface.

2. Ge

Six sets of angle-resolved XPS data were collected on (111)-oriented samples. Ultraviolet photoelectron spectroscopy (UPS)[22] and electron-energy-loss spectroscopy (EELS)[23] measurements on (111) samples have indicated the presence of a surface state a few tenths of an eV below E_v^{Ge}. XPS data were collected for $\phi = 0°$, 30°, and 60°. Analyses of these data (Sec. III A 3) indicated that the surface state was substantially affecting the E_v^{Ge} determination. Thus four additional sets of XPS data were collected on (110)-oriented samples for $\phi = 0°$ or 90°. Although the Ge(110) surface has been studied by LEED,[9,24] and possible surface structures have been considered,[25] little is known about the electronic structure of this surface.

III. ANALYSIS OF XPS DATA

The objective of our XPS data analysis is the precise determination of $E_{\mathrm{CL}}^x - E_v^x$ and the spin-orbit–split components $E_{3d_{3/2}}^x - E_v^x$ and $E_{3d_{5/2}}^x - E_v^x$ shown schematically in Fig. 2(a). This depends on locating the position of E_v^x in the XPS data with greater accuracy than has been generally attempted previously. We shall present a new method, based on fitting an instrumentally broadened theoretical valence-band density of states (VB DOS) to the XPS valence-band data in the region around E_v^x by using the method of least squares. Also in this section we discuss the analysis of the core-level energy positions, the resolution of the core-level spin-orbit–split components, and the limits of precision associated with the data analysis.

A. Location of E_v^x in the XPS data

The location of E_v^x in XPS data is complicated, even in the absence of occupied surface states, due to the slowly varying photoelectron signal in this energy region. For

semiconductors, methods such as extrapolating the tangent line to the leading edge of the photoelectron valence-band spectrum back to the energy axis and defining the slope intercept as E_v^x have been used.[26,27] For metallic gold, the location of the inflection point in the XPS data has been used to define E_v (Refs. 28 and 29); while the inflection-point location method is appealing for metals with a partially filled valence band which has a slowly varying density of states near E_v, it is not appropriate for semiconductors. A major uncertainty is introduced into the determination of $E_{\rm CL}^x - E_v^x$ for semiconductors by the extrapolation procedure used to locate E_v^x in the XPS data.

We have developed a method to obtain the position of E_v^x in XPS data by modeling a portion of the XPS valence-band spectrum in the region of E_v^x with an instrumentally broadened theoretical valence-band density of states $N_v(E)$, defined so that

$$N_v(E)=\int_0^\infty n_v(E')\sigma(E',h\nu)f(E')g(E-E')dE' . \quad (2)$$

In Eq. (2), $n_v(E')$ is a theoretical valence-band density of states. For Ge and GaAs data analyses we have employed the nonlocal pseudopotential VB DOS's of Chelikowsky and Cohen.[30] The next factor in Eq. (2) is the cross section or transition probability for photoionization

$$\sigma(E',h\nu) \propto |\langle \psi_f | P_{fi} | \psi_i \rangle|^2 ,$$

where P_{fi} is the transition operator between final- and initial-state wave functions ψ_f and ψ_i. In experiments reported here, $h\nu$ is 1486.6 eV, so that the density of available final states is sufficient for excitation of all initial states.

The factor $f(E')$ in Eq. (2) is the Fermi function and represents the effect of thermal broadening on the VB DOS. Since the integration is over the filled valence bands of a moderately doped semiconductor, the Fermi factor $f(E')$ is set equal to unity. The last factor in Eq. (2) is the instrumental resolution function $g(E)$ which is separately determined as discussed in Sec. III A 1.

To determine E_v^x from the XPS GaAs and Ge data, an energy interval extending from a few eV above E_v^x to ≈ 1 eV below E_v^x was analyzed. After setting $f(E')=1$, the remaining integral in Eq. (2) is recognized as a moving average of $n_v(E')\sigma(E',h\nu)$ over an interval roughly the full width at half maximum (FWHM) of the instrumental response function $g(E')$ and centered at energy E. If $\sigma(E',h\nu)$ is nearly constant when E' changes by no more than the FWHM of g, while $n_v(E')$ may vary by a large fraction over the same interval, then approximately,[31]

$$N_v(E)=\langle n_v\sigma\rangle \cong \langle n_V\rangle_E\langle\sigma\rangle_E . \quad (3)$$

The assumption that the photoelectric valence-band cross section varies more slowly than the VB DOS over the width of g is supported by both theoretical[32–34] and experimental results.[35] Near E_v^x the orbital character of the wave functions is essentially p type and $\langle\sigma\rangle_E$ reduces to the constant cross section σ_p of p electrons. It follows from Eq. (3) that near E_v^x $N_v(E)$ is approximately

$$N_v(E)=\sigma_p\int_0^\infty n_v(E')g(E-E')dE' . \quad (4)$$

The position of E_v^x in the XPS data was determined by fitting $N_v(E)$ to the XPS valence-band data in the energy region around E_v^x by the method of least squares; thus E_v^x corresponds to $N_v(0)$. The fitting procedure involved three parameters, a scale factor S, the position of the valence-band edge E_v^x, and a constant random background B. The XPS spectral intensity $I(E)$ was assumed to have the form

$$I(E)=SN_v(E-E_v)+B . \quad (5)$$

In order to compare Eq. (5) with the experimental XPS data $I_{\rm XPS}(E)$, both $N_v(E)$ and $I_{\rm XPS}(E)$ were normalized so that the first peak below E_v^x corresponded to a peak height of unity. The parameters E_v^x, S, and B are then adjusted until the total error $\mathscr{E}$,

$$\mathscr{E}^2=\int_{E_{\rm min}}^{E_{\rm max}}[I_{\rm XPS}(E)-I(E)]^2dE , \quad (6)$$

is minimized for the fitting interval between $E_{\rm min}$ and $E_{\rm max}$. In practice, E_v^x computed by minimizing Eq. (6) may be a function of $E_{\rm max}$. This complication will be discussed in relation to analyses of specific GaAs and Ge XPS data (Secs. III A 2 and III A 3). Finally we observe that when the experimental data $I_{\rm XPS}(E)$ closely resemble the shape of the instrumentally broadened VB DOS $N_v(E)$ up to $E_{\rm max}$, the scale factor S in Eq. (5) can be replaced by $1-B$ without sacrificing the quality of the fit.

1. *Determination of the spectrometer response function*

Our experimental results show that the shape of an experimental XPS spectrum around E_v^x is primarily controlled by $g(E)$. Therefore, the ability to determine an accurate analytic closed-form expression for the instrumental response function $g(E)$ plays an important role in determining precise values for the core-level to valence-band-edge binding-energy differences indicated in Fig. 2(a).

Experimentally observed Au $4f_{7/2}$ and Au $4f_{5/2}$ line shapes had FWHM of $\sim$0.86 eV. Each of these lines $W_{{\rm Au}\,4f_x}$ is related to $g(E)$ by

$$W_{{\rm Au}\,4f_x}(E)=A_x\int_{-\infty}^\infty g(E-E')L(E')dE' , \quad (7)$$

where A_x is a scale factor and $L(E')$ is a Lorentzian line shape (FWHM$=0.317\pm0.010$ eV),[36] which represents the inherent lifetime broadening of the Au $4f$ levels. An experimental characteristic of the gold $4f$ core levels is that after subtraction of a background function which is proportional to the integrated photoelectron peak area from the raw XPS data,[28] they are nearly symmetric and Gaussian around the peaks and Lorentzian in the tails. To represent the background-subtracted $W_{{\rm Au}\,4f}(E)$ data analytically requires a function that is Gaussian in the core and Lorentzian in the tail. Voigt functions, formed by folding Gaussians with Lorentzians, have precisely this property, and have already been suggested as being useful for the analysis of experimental XPS line shapes.[37]

In terms of the Voigt function

$$U(SE,b)=\frac{b}{S\pi^{3/2}}\int_{-\infty}^\infty \frac{e^{-S^2x^2}}{(b/S)^2+(E-x)^2}dx \quad (8)$$

of unit integrated area, the Au $4f$ spin-orbit–split doublet is represented as

$$W_{\mathrm{Au}\,4f}=A_1 U(S(E-E_1),b)+A_2 U(S(E-E_2),b)\ . \tag{9}$$

The parameters A_1, A_2, E_1, E_2, S, and b are obtained by fitting Eq. (9) to the background-subtracted XPS Au $4f$ core lines by using the method of least squares. A fit such as that shown in Fig. 4 is obtained each time a semiconductor core-level to valence-band-maximum binding-energy difference is measured in order to determine the instrumental response function $g(E)$ appropriate to the particular measurement in question.

The integral equation (7) for $g(E)$ can be solved exactly to yield the following closed-form analytic expression for the instrumental response function

$$g(E)=U(SE,b-K)\ . \tag{10}$$

The parameters S and b in Eq. (10) are obtained from the least-squares fit in Eq. (9), and K is determined from the inherent (0.317 eV) (Ref. 36) linewidth (Γ_{FWHM}) of the lifetime-broadened Au $4f$ core levels through the relation

$$K=S(\Gamma_{\mathrm{FWHM}})/2\ . \tag{11}$$

Phonon broadening of the Au $4f$ lines used to determine $g(E)$ was calculated following Citrin *et al.*[38] and was found to affect the $g(E)$ width by less than 0.01 eV; a similar result was reported by Citrin *et al.*[36]

2. *Results for GaAs*

The Ga $3d$ and As $3d$ core-line centers (defined as the midpoint of the peak width at half of the peak height) were determined from the XPS data after a background function, which is proportional to the integrated photoelectron peak area, was subtracted to correct for the effect of inelastic photoelectron scattering. This procedure made it unnecessary to resolve spin-orbit splitting of the core lines to obtain high-precision peak positions. The position of E_v^{GaAs} was determined in the same spectrum by using the fitting procedure outlined in Sec. III A.

Figure 5 shows the position of the E_v^{GaAs} measured relative to the center of the Ga $3d$ core level as a function of E_{max} for three angle-resolved sets of XPS measurements made on GaAs(110) surfaces. The azimuthal angles $\phi=0°$, 35°, and 90° are defined in Fig. 3. The least-squares analyses for the values of $E_v^{\mathrm{GaAs}}(E_{\mathrm{max}})$ and B, which minimize Eq. (6), were performed by using Marquardt's algorithm.[39] The error bars shown in Fig. 5 represent the 95% central confidence interval[40] for each least-squares value of $E_{\mathrm{Ga}\,3d}^{\mathrm{GaAs}}-E_v^{\mathrm{GaAs}}(E_{\mathrm{max}})$. Convergence to a common value of $E_{\mathrm{Ga}\,3d}^{\mathrm{GaAs}}-E_v^{\mathrm{GaAs}}=18.83$ eV occurs for $E_{\mathrm{max}}\lesssim 1.0$ eV below E_v^{GaAs}.

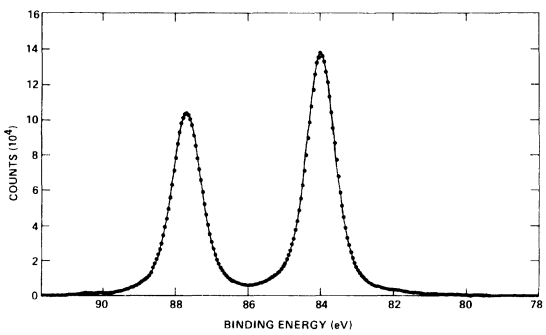

FIG. 4. Least-squares fit (solid curve) of the sum of two Voigt functions to the Au $4f_{5/2}$ and Au $4f_{7/2}$ background-subtracted (closed circles) Au $4f$ XPS spectrum.

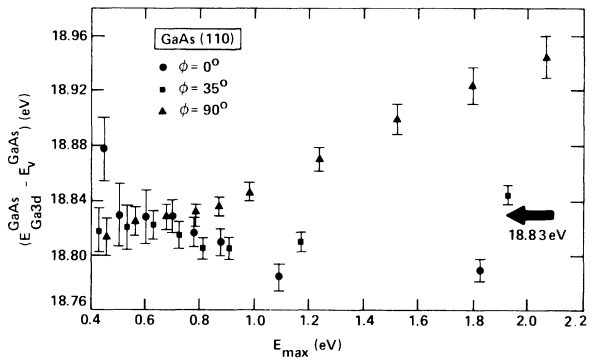

FIG. 5. Position of the GaAs valence-band maximum E_v^{GaAs} measured relative to the center of the Ga $3d$ core level as a function of the end point E_{max} of the fitting interval for azimuthal angles of 0°, 35°, and 90° defined in Fig. 3.

The variation of $E_{\mathrm{Ga}\,3d}^{\mathrm{GaAs}}-E_v^{\mathrm{GaAs}}$ with ϕ and with E_{max} can be explained in terms of occupied states associated with the GaAs(110) surface. Detailed analyses of the relaxed GaAs(110) surface electronic structure have been performed.[19–21] Although the surface electronic structure is quite sensitive to precise details of the geometry, in general, the theoretical calculations place the highest-lying energy peaks in the local density of states between 0.5 and 1.5 eV below E_v^{GaAs}. Experimental results[41,42] place the highest-lying surface-state peak at ≈ 1 eV below E_v^{GaAs} for the GaAs(110) surface. Thus for our spectrometer response function (see Sec. III A 1) it might be expected that the XPS valence-band data within ≈ 1 eV of E_v^{GaAs} would not contain substantial surface-state contributions. The unique value of $E_{\mathrm{Ga}\,3d}^{\mathrm{GaAs}}-E_v^{\mathrm{GaAs}}$ for $E_{\mathrm{max}}\lesssim 1.0$ eV appears to confirm this view.

The orbital character of the GaAs(110) surface states has been considered in detail. Chadi's calculations[19] indicate that the highest-lying surface state consistent with the 27° rotational relaxation model[15] has a predominantly p_y-orbital character, while the bond relaxation model[16] has a predominantly p_z character, with about equal amounts of p_x and p_y. In describing the p-derived orbital symmetries of the surface states, the $\vec{x}$ direction is parallel to (110), the $\vec{y}$ direction is parallel to (001), and the $\vec{z}$ direction is parallel to $(1\bar{1}0)$.

Zunger[43] has pointed out that the upper As surface state has about 20% d character, and that there is a certain amount of arbitrariness in the assignment of atomic-orbital character to surface states. Experimental results[44,45] suggest that the highest-lying surface states have predominantly p_y character (rather than p_x).

The photoelectron cross section σ is given following Gelius[14] as

$$\sigma \propto |\langle p\,|\,PW(\vec{k})\rangle|^2\ , \tag{12}$$

the square of the absolute value of the overlap between an orbital involved in the photoemission and the plane wave

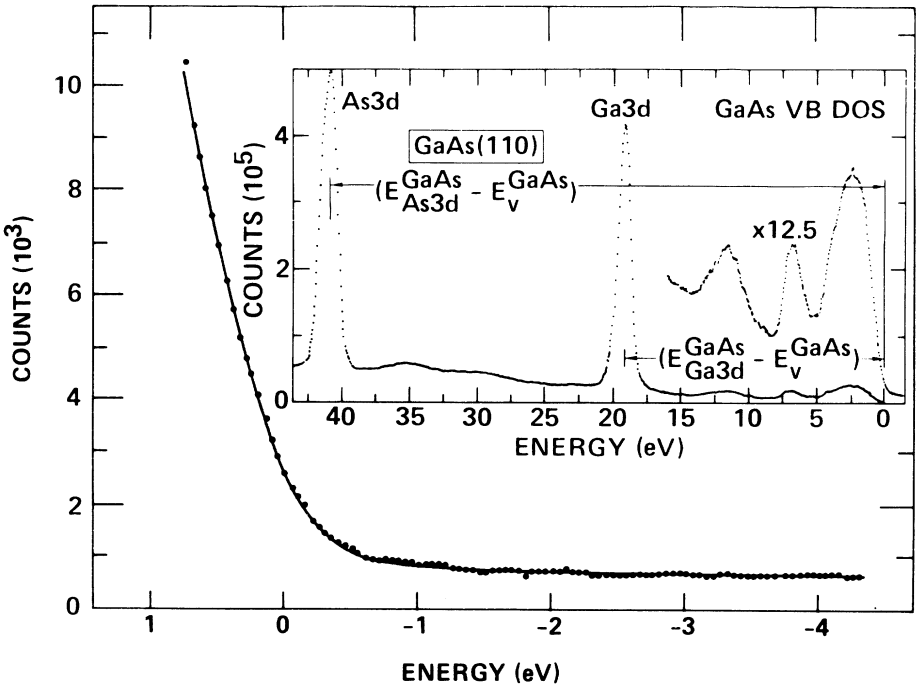

FIG. 6. Least-squares fit of the instrumentally broadened theoretical VB DOS (solid curve) to XPS data (dots) in the region of the valence-band maximum for GaAs. Inset shows the XPS spectrum which contains the VB DOS and the outermost core levels. The energy scale is zero at the valence-band maximum.

$PW(\vec{k})$ representing the free electron; $\vec{k}$ denotes the wave vector for the photoelectron. Referring to Fig. 3, for $\phi=0°$ and 90°, $\vec{e}$ is orthogonal to $\vec{y}$ and $\vec{x}$, respectively. Thus one would expect the maximum photoelectron cross-section contribution, Eq. (12), to the XPS valence-band data from predominately p_y-character surface states when $\phi=90°$. This could account for the enhanced sensitivity of the $E^{GaAs}_{Ga\,3d}-E^{GaAs}_v$ determination to the fitting interval for $\phi=90°$ data as noted in Fig. 5.

Figure 6 shows the least-squares fit of the instrumentally broadened $N_v(E)$ (solid curve) to XPS data (dots) in the region near E^{GaAs}_v. The inset in Fig. 6 shows the XPS spectrum which contains the valence band and the Ga 3*d* and As 3*d* core levels. The energy scale is zero at E^{GaAs}_v as discussed in Sec. III A. By analyzing six sets of GaAs(110) data as described here, the XPS measured values for $E^{GaAs}_{Ga\,3d}-E^{GaAs}_v$ and $E^{GaAs}_{As\,3d}-E^{GaAs}_v$ are 18.83 and 40.75 eV, respectively.

3. *Results for Ge*

The Ge 3*d* core line center was determined from XPS data in the same manner that the Ga 3*d* and As 3*d* line centers were determined (see Sec. III A 2). Also, the position of E^{Ge}_v was determined by the fitting procedure given in Sec. III A.

Figure 7(a) shows the results of analyzing three angle-resolved sets of data taken on the Ge(111) surface, and two additional sets of data for the Ge(110) surface. The azimuthal angle ϕ is defined in Fig. 3. The error bars are defined as in Fig. 5. UPS (Ref. 22) and EELS (Ref. 23) measurements on the Ge(111) 2×8 surface have indicated the presence of a high-lying surface state a few tenths of an eV below E^{Ge}_v. This surface state has been associated with a dangling-bond state. Theoretical calculations[46] on the relaxed Ge(111) surface have placed a dangling-bond state, which has p_z-orbital character within 0.1 eV of E_v [the $\vec{z}$ direction is parallel to (111)].

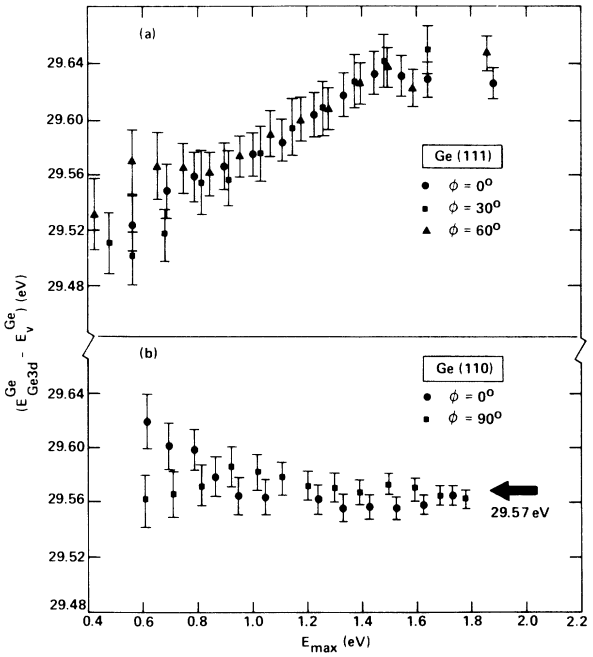

FIG. 7. Position of the Ge valence-band maximum E^{Ge}_v measured relative to the center of the Ge 3*d* core level as a function of the end point E_{max} of the fitting interval. Results are shown for azimuthal angles (Fig. 3) of 0°, 30°, and 60° on the (111) crystal face and 0° and 90° on the (110) crystal surface.

ed that this surface state would contribute substantially to the photoelectron signal in the vicinity of E_v^{Ge}, and that because of the p_z-orbital character of this state, variations of ϕ would have little effect on the ratio of surface to bulk emission in the photoelectron signal near E_v^{Ge}. The Ge(111) XPS data collected for $\phi=0°$, 30°, and 60° and analyzed as shown in Fig. 7(a) seem to confirm this view. The analysis does not produce a satisfactory determination of $E_{Ge\,3d}^{Ge}-E_v^{Ge}$ because of the monotonic variation of $E_{Ge\,3d}^{Ge}-E_v^{Ge}$ with E_{max}.

In order to determine $E_{Ge\,3d}^{Ge}-E_v^{Ge}$, angle-resolved Ge(110) data were analyzed as shown in Fig. 7(b). The relatively constant value of $E_{Ge\,3d}^{Ge}-E_v^{Ge}$ independent of E_{max} and ϕ suggests that any filled Ge(110) surface states below E_v^{Ge} are either very weakly localized near the surface or lie well outside the energy interval analyzed, since it is unlikely that σ for such (110) surface states would be independent of ϕ.

Figure 8 shows a least-squares fit of $N_v(E)$ (solid line) to Ge(110) XPS data (dots) in the region of E_v^{Ge}. The inset in Fig. 8 shows the XPS spectrum containing the valence band and the Ge 3d core level. The energy scale is zero at E_v^{Ge}. By analyzing four sets of Ge(110) data, the XPS measured value for $E_{Ge\,3d}^{Ge}-E_v^{Ge}$ was 29.57 eV.

B. Surface chemical shifts

The chemical shifts of surface atoms relative to bulk binding energies have recently been measured for several semiconductors.[18,47–49] In particular, for the GaAs(110) surface, it is observed[18] that the surface Ga 3d level is shifted to larger binding energy by $\Delta E_B=0.28$ eV, while the As 3d level is shifted to smaller binding energy by $\Delta E_B=-0.37$ eV. For the Si(111) 2×1 surface, surface chemical shifts of $\Delta E_B=-0.59$ and $+0.30$ eV have been reported[47] for the Si 2p level. Both the GaAs(110) and Si(111) 2×1 surface measurements indicate that the surface chemical shifts are predominantly associated with initial-state charge transfer in the outermost atom layer. It has been emphasized[50] that sizable surface chemical shifts may influence XPS measured core-level binding energies.

The apparent shift of the XPS measured $(E_{CL}^x-E_v^x)_{XPS}$ from the bulk value due to surface chemical shifts can be estimated with good accuracy if knowledge of these shifts is available. A small correction can then be applied to obtain the bulk $(E_{CL}^x-E_v^x)_b$ values. We have used the measured[18] GaAs(110) surface chemical shifts to estimate corrections to our Ga 3d and As 3d XPS binding-energy measurements. The electron escape depth λ has been measured in Ge for an electron kinetic energy E_k of 1228 eV as $\lambda(1228\text{ eV})=24.2\pm2$ Å (Ref. 8); for $E_k>200$ eV, it was found that $\lambda\propto E_k^{0.56}$. Extrapolating this result to $E_k=1450$ eV, which is more appropriate for the Ga 3d, Ge 3d, and As 3d levels studied in this work, yields $\lambda(1450\text{ eV})=26.6\pm2.2$ Å. This result is in good agreement with an earlier, although less precise, measurement of $\lambda(1404\text{ eV})=29\pm4$ Å which was obtained for amorphous Ge.[51] The GaAs(110) interplanar spacing is 2.00 Å, and the photoelectron-emission direction relative to the surface normal is 51.5°. Assuming an ideally flat surface, approximately 11.4±0.9 % of the Ga 3d and As 3d photoelectron signals originate from the surface layer. The apparent

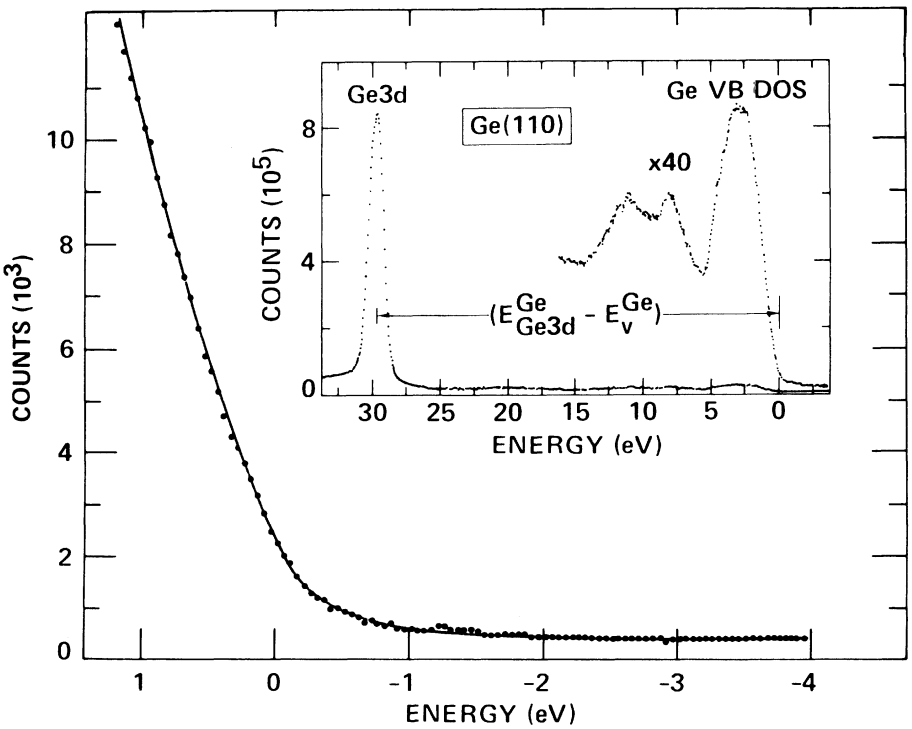

FIG. 8. Least-squares fit of the instrumentally broadened theoretical VB DOS (solid curve) to XPS data (dots) in the region of the Ge valence-band maximum. Inset shows the XPS spectrum which contains the VB DOS and the Ge 3d core level. The energy scale is zero at the valence-band maximum.

shift in the Ga $3d$ and As $3d$ core levels caused by the surface chemical shifts of $\Delta E_B = +0.28$ and -0.37 eV, respectively, was estimated by summing the experimentally observed line shapes with a second component, which was shifted in energy by the appropriate surface chemical shift, and had an intensity scaled to represent 11.4% of the total signal. The estimated shifts of the Ga $3d$ and As $3d$ line centers due to surface chemical shifts are $+0.030$ and -0.035 eV, respectively. When these shifts are subtracted from the measured $(E^x_{CL}-E^x_v)_{XPS}$ values, the $(E^x_{CL}-E^x_v)_b$ values for GaAs are 18.80 and 40.79 eV for $(E^{GaAs}_{Ga\,3d}-E^{GaAs}_v)_b$ and $(E^{GaAs}_{As\,3d}-E^{GaAs}_v)_b$, respectively.

Surface chemical shifts have not yet been studied on Ge(110) surfaces, however, the magnitudes of surface chemical shifts observed on Ge(111) surfaces[48] are similar to those observed on the GaAs(110) (Ref. 18) and Si(111) surfaces.[47–49] If surface chemical shifts on the Ge(110) surface are predominantly associated with initial-state charge transfer, one might expect that the major effect on the XPS-measured Ge $3d$ photoelectron line would be a small-line broadening with a very modest line-center shift. The Si $2p$ surface chemical shifts measured on the Si(111) 2×1 surface[47] may be a somewhat analogous situation; from a simple first moment type of argument, one can estimate a centroid shift of -0.017 eV for the Si $2p$ line for our experimental arrangement.

The surface chemical-shift correction to $(E^x_{CL}-E^x_v)_{XPS}$ is not very sensitive to the exact photoelectron line shape. From a first-moment calculation, one would estimate apparent Ga $3d$ and As $3d$ line centroid shifts of $+0.032$ and -0.042 eV for our experimental geometry. This suggests that a surface chemical-shift correction can be made with good accuracy (assuming that these shifts are known for a particular surface).

C. Resolution of spin-orbit–split core-level to valence-band-edge binding-energy differences

The operational definition of the core-level binding energy as the energy corresponding to the midpoint of the peak width at half the core-level peak height is convenient because core lines are prominent in XPS spectra and the line centers are easy to locate accurately. However, the width of the core level is not only dependent on intrinsic broadening mechanisms such as lifetime broadening and phonon broadening, but is also dependent on the broadening introduced by the spectrometer response function.

In order to eliminate the effect of spectrometer broadening and to obtain instrument-independent core-level to E_v binding-energy differences, it is necessary to refer binding-energy measurements to the $3d_{3/2}$ and $3d_{5/2}$ spin-orbit–split components of the $3d$ core levels. These instrumentally independent core-level to E_v binding-energy differences should be true semiconductor bulk properties, and should be more easily compared with other experimental results.

In order to resolve the spin-orbit–split $3d_{3/2}$ and $3d_{5/2}$ core-line components, it is assumed that the instrumentally broadened experimental $3d$ core line $W^x_{x\,3d}(E)$ is representable as a linear combination $\tilde{W}^x_{x\,3d}(E)$ of two Voigt functions, $U(SE,b)$, defined in Eq. (8) and separated from one another by the spin-orbit splitting Δ_{so},

$$\tilde{W}^x_{x\,3d}(E)=A_1U(S(E-E_1),b_1)+A_2U(S(E-E_2),b_2)\ , \tag{13}$$

where

$$\Delta_{so}=(E_1-E_2)\ . \tag{14}$$

The parameters A_1, A_2, E_1, S, b_1 and b_2 are determined by the method of least squares[39] by adjustment until the total error given by

$$\mathscr{E}^2=\int_{E_{initial}}^{E_{final}}[W^x_{x\,3d}(E)-\tilde{W}^x_{x\,3d}(E)]^2dE \tag{15}$$

is minimized. The integration interval $E_{final}-E_{initial}$ in Eq. (15) is large enough to include nearly the entire instrumentally broadened core line. Figures 9(a)–9(c) show typical least-squares fits of Eq. (13) to Ga $3d$, Ge $3d$, and As $3d$ core lines, respectively. The line center is defined as zero energy in the figure. The intensity ratio $I(\frac{3}{2})/I(\frac{5}{2})$ has a theoretical value $[2\times(\frac{3}{2})+1]/[2\times(\frac{5}{2})+1]$ equal to 0.67 in approximate agreement with the intensity ratios determined from the individual spin-orbit–split line components which are also shown in Fig. 9.

The spin-orbit splittings Δ_{so} used to analyze these data are given in Table I and were determined from other data such as XPS results or in the case of As $3d$ from interpolation between other high-resolution electron spectroscopy data.[7,18] The binding energies for the spin-orbit–split components relative to the line centers for Ga $3d$ and As $3d$ core lines in GaAs and for the Ge $3d$ core line in Ge are also given in Table I.

D. Precision analysis

In this section we consider factors which affect the precision of XPS core-level binding-energy measurements.

TABLE I. Binding energies of spin-orbit components relative to line centers in eV.

Core level	Spin-orbit splitting	Binding energy relative to line center
Ga $3d_{5/2}$ (GaAs)	0.43	-0.17
Ga $3d_{3/2}$ (GaAs)		$+0.26$
Ge $3d_{5/2}$ (Ge)	0.55	-0.21
Ge $3d_{3/2}$ (Ge)		$+0.34$
As $3d_{5/2}$ (GaAs)	0.71	-0.30
As $3d_{3/2}$ (GaAs)		$+0.41$

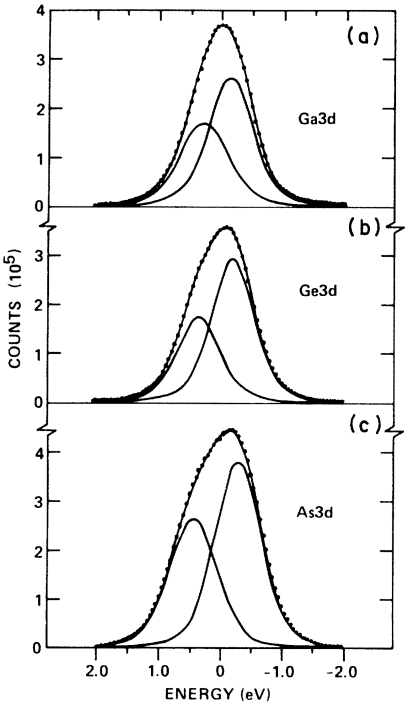

FIG. 9. Resolution of the spin-orbit–split Ga, Ge, and As $3d_{3/2}$ and $3d_{5/2}$ core-level components by means of a least-squares fit of the sum of two Voigt functions to the background-subtracted $3d$-core line shapes.

1. Band bending

Free-surface band bending could affect the accurate XPS determination of core-level to valence-band maximum binding-energy differences for heavily doped materials. When the surface Fermi-level pinning position is known, it would be possible to minimize this complication by a judicious choice of bulk doping density. In general, this complication should be more severe for wide-band-gap than for narrow-band-gap semiconductors.

For n-type GaAs, a typical surface band bending is 0.8 eV.[52,53] Therefore, as a worst-case estimate for the effect of band bending on the core-level to E_v^x binding-energy difference, a simple calculation was carried out to determine the shift of the Ga $3d$ core-level center for a surface potential $V_{ss}=0.8$ V, a doping density $N_D=1\times10^{17}$ cm^{-3}, a dielectric constant $\epsilon_s=12$, and an escape depth equal to 26.6 Å.[8] In the depletion approximation, the potential, $V(x)$, within a surface-depletion region of width W, is given by

$$V(x)=E_m[x-(x^2/2W)]\ , \tag{16}$$

where the maximum electric field at the surface is $|E_m|=qN_DW/\epsilon_s$ and $W=(2\epsilon_sV_{ss}/qN_D)^{1/2}$; q is the electronic charge. For our measurements the electron-emission direction relative to the sample surface normal was 51.5°; this angle decreases the effective sampling depth and its effect was included in the calculation. Assuming an ideally smooth surface, photoelectrons generated at a depth x below the surface are attenuated exponentially as

$$I(x)=I_0\exp(-x/\lambda\cos\theta)\ , \tag{17}$$

where I_0 is the unattenuated intensity emitted from the surface at $x=0$. Thus the envelope of the core line $M(E)$ which is shifted in energy due to band bending is given by

$$M(E)=\int_0^\infty m(E-V(x))\exp(-x/\lambda\cos\theta)dx\ , \tag{18}$$

where $m(E)$ is the core-level line shape observed at the surface. The calculations utilized the experimentally observed XPS Ga $3d$ line shape for $m(E)$. For the conditions specified above, the total shift of the line center was 0.014 eV. Thus for the moderate doping densities of the samples utilized herein, band bending affects the observed core-level center by less than 0.01 eV. A smaller shift in the observed E_v^x would also be expected due to band bending. Because the two shifts would be in the same direction, they would tend to cancel.

2. Accuracy of the instrumental response function

The method used to determine g was outlined in Sec. III A 1. The typical precision in the least-squares procedure used to model the Au $4f$ line shapes for the purposes of determining g produced an uncertainty in the Voigt-function FWHM of about 0.01 eV. The instrumental response function is determined by deconvolving a Lorentzian curve with $\Gamma_{\rm FWHM}=0.317\pm0.010$ eV (Ref. 36) (determined by the Au $4f$ final-state lifetime) from the Voigt function used to model the Au $4f$ line shape. An uncertainty in the deconvolved Lorentzian curve of 0.01 eV would produce an additional uncertainty in the FWHM of the instrumental response function of about 0.006 eV leading to a total uncertainty in the FWHM of the instrumental response function of ≈0.012 eV.

3. Choice of the theoretical VB DOS

As a test of the sensitivity of the core-level to valence-band-maximum binding-energy determinations to the particular theoretical (VB DOS) $n_v(E)$ used in Eq. (4), computations were performed for both local[54] and nonlocal[30] pseudopotential VB DOS's. The latter includes the effects of spin-orbit splitting of the valence band, and also represents valence bandwidths more accurately.[30] Computational results show that the difference between local[54] and nonlocal[30] pseudopotential VB DOS's in Eq. (4) amounts to less than a 0.01-eV change in the apparent position of E_v^x. The effect of the spin-orbit splitting at the valence-band edge, which amounts to 0.34 and 0.29 eV in GaAs and Ge, respectively,[55] was not resolvable in the experiments reported here.

4. Effects of background subtraction

A background function which was proportional to the integrated photoelectron peak area was subtracted from all core-level peaks to remove approximately the contribution from inelastically scattered photoelectrons from the XPS spectra. It was found that this correction shifted the apparent $E_{\rm CL}^x$ position by ≤0.01 eV. The effect of background on the E_v^x determination was also investigated by subtracting a similar background function from the XPS

valence-band data. By determining E_v^x (with the procedure outlined in Sec. III A) from XPS valence-band data both with and without the background correction applied, it was observed that the apparent E_v^x position was only shited by ~ 0.005 eV due to background effects.

5. *Precision limits*

In Secs. III D 1—III D 4 several factors which affect the limits of precision on XPS $E_{\mathrm{CL}}^x - E_v^x$ measurements have been discussed. These factors are now combined to obtain precision limits for the experimentally measured binding-energy differences reported in this paper.

As noted in Sec. II D, the precision in determining a core-level center from the experimental data was about 0.005 eV. Possible effects of band bending within the XPS sampling depth were shown (Sec. III D 1) to introduce an uncertainty of less than 0.01 eV in the apparent core-level position. The background-subtraction procedure used in analyzing the core-level data produced an apparent energy shift of ≤ 0.01 eV (Sec. III D 4), which provides an estimate of the uncertainty caused by background effects. Combining these three uncertainties leads to an uncertainty in determining the core-level center from XPS data of ≤ 0.015 eV. To remove approximately the effect of surface chemical shifts from the XPS-measured core-level center position, a correction was applied (see Sec. III B). If we assume that the accuracy of the surface chemical-shift determination[18] is ± 0.05 eV and consider the uncertainty in λ of ± 2.2 Å (see Sec. III B), the uncertainty in the surface chemical-shift correction is less than 0.006 eV. Thus the total uncertainty in determining the core-level center for bulk material is ≤ 0.016 eV.

Uncertainty in g affects the uncertainty in the determination of E_v^x from the experimental data. By fitting data near E_v^x with theoretical functions obtained by folding VB DOS's with Voigt-function approximations to g which spanned the range of uncertainty in g (see Sec. III D 2), it was determined that the uncertainty in g produced a 0.014-eV uncertainty in determining E_v^x. The choice of theoretical density of states in the valence-band-edge modeling procedure was shown to introduce a variation in the apparent E_v^x position of less than 0.01 eV (Sec. III D 3). The precision of the least-squares-fitting procedure used to locate E_v^x in the experimental data was typically 0.005 eV, and the estimated uncertainty due to background effects is ~ 0.005 eV (Sec. III D 4). Thus the total uncertainty in determining the position of E_v^x in the experimental data is ≤ 0.019 eV.

By combining the uncertainties in determining the core-level center and E_v^x from the experimental data, the uncertainty in the $E_{\mathrm{CL}}^x - E_v^x$ values is estimated as ≤ 0.025 eV. The spectrometer energy scale is calibrated to 0.02% (Sec. II B). The uncertainty in this calibration introduces an uncertainty in determining $E_{\mathrm{CL}}^x - E_v^x$ which increases with increasing core-level binding energy. The As $3d$ core level had the largest binding energy of core levels studied in this work, and therefore provides a worst-case estimate. Including the uncertainty due to spectrometer calibration leads to a total uncertainty in the core-level to E_v^x binding-energy difference of ≤ 0.026 eV.

The curve-fitting procedure used to determine the energy positions of the core-level spin-orbit components is discussed in Sec. III C. The precision of the fitting procedure was less than 0.01 eV. The uncertainty in the magnitude of the spin-orbit splitting for Ga $3d$, Ge $3d$, and As $3d$ core levels is about ± 0.05 eV (Refs. 7 and 18) and thus the uncertainty of each spin-orbit—split component relative to the line center would be ~ 0.035 eV. The total uncertainty in determining the spin-orbit components relative to the line center is therefore about 0.036 eV. Combining this uncertainty with the uncertainty in the measurement of the line-center position leads to a total uncertainty for the spin-orbit components to E_v^x binding-energy differences of ≤ 0.044 eV.

IV. SUMMARY

A procedure has been developed to measure semiconductor core-level to valence-band maximum binding-energy differences with greater precision than has been previously attempted. This procedure involves analyzing an XPS spectrum in which both the core-level and valence-band data have been collected simultaneously. The position of E_v^x in the XPS spectrum is determined by least-squares-fitting a theoretical VB DOS, which has been broadened by the instrumental response function to data in a limited energy region near E_v^x. The instrumental response function is determined from analysis of XPS-measured Au $4f$ core-level data. The effects of occupied surface states on the measurements are determined by analyzing angle-resolved data obtained from samples with known crystallographic orientations. The spin-orbit—split components of particular core levels are resolved by employing the method of least squares.

Core-level to E_v^x binding-energy differences have been determined for Ga $3d$ and As $3d$ in GaAs, and for Ge $3d$ in Ge. The experimental results and limits of precision are

TABLE II. Core-level to E_v^x binding-energy differences in eV. The absolute value of the uncertainty in the least significant figure is indicated in parentheses.

Semiconductor surface	Core level	$(E_{\mathrm{CL}}^x - E_v^x)_{\mathrm{XPS}}$	$(E_{\mathrm{CL}}^x - E_v^x)_b$	$(E_{3d_{5/2}}^x - E_v^x)_b$	$(E_{3d_{3/2}}^x - E_v^x)_b$
GaAs(110)	Ga $3d$	18.83(3)	18.80(3)	18.63(4)	19.06(4)
	As $3d$	40.75(3)	40.79(3)	40.47(4)	41.18(4)
Ge(110)	Ge $3d$	29.57(3)	29.57(3)[a]	29.36(4)	29.91(4)

[a]The Ge $3d$ surface chemical shifts for the Ge(110) surface are unknown. From the argument given in Sec. III B there should be little difference between the XPS measured and bulk values of $E_{\mathrm{CL}}^{\mathrm{Ge}} - E_v^{\mathrm{Ge}}$.

summarized in Table II. This table includes the XPS-measured values of the core-level center to E_v^x binding-energy differences $(E_{CL}^x - E_v^x)_{XPS}$ and the corresponding bulk semiconductor values $(E_{CL}^x - E_v^x)_b$, which have been corrected for surface chemical-shift effects. Also included in the table are the bulk semiconductor values of binding energies for the spin-orbit–split components of the core levels relative to E_v^x.

The value of $(E_{Ga\,3d}^{GaAs} - E_v^{GaAs})_{XPS}$ is in good agreement with previous literature that reported results of 18.9 ± 0.1 (Refs. 4 and 6) and 18.82 ± 0.15 eV.[5] The value of $(E_{Ge\,3d}^{Ge} - E_v^{Ge})_{XPS}$ is in rather poor agreement with the previously reported result of 29.0 ± 0.1 eV.[6] The binding energies of the Ga $3d$ and As $3d$ spin-orbit–split components relative to E_v^{GaAs} have recently been measured[18] as $E_{Ga\,3d_{5/2}}^{GaAs} - E_v^{GaAs} = 18.60$ eV, $E_{Ga\,3d_{3/2}}^{GaAs} - E_v^{GaAs} = 19.04$ eV, $E_{As\,3d_{5/2}}^{GaAs} - E_v^{GaAs} = 40.37$ eV, and $E_{As\,3d_{3/2}}^{GaAs} - E_v^{GaAs} = 41.07$ eV. Considering the precision limits of the experiments, these results are in very good agreement with the results reported here. Earlier reported[7] binding energies for the spin-orbit–split components of Ge $3d$ relative to E_v^{Ge} are $E_{Ge\,3d_{5/2}}^{Ge} - E_v^{Ge} = 29.1$ eV, and $E_{Ge\,3d_{3/2}}^{Ge} - E_v^{Ge} = 29.65$ eV; these values are not in as good agreement with our present results. Although the origin of the discrepancy cannot be identified with certainty, the earlier measurements were obtained on Ge(111) surfaces, and the occupied surface-state emission may have complicated the determination of E_v^{Ge}. We note from our data in Fig. 7 that if Ge(111) data were analyzed only in a small interval near E_v^{Ge}, a substantially lower $E_{Ge\,3d}^{Ge} - E_v^{Ge}$ would be obtained.

We have previously discussed[3] the applications of photoelectron spectroscopy for determining semiconductor band bending, Schottky-barrier heights, and heterojunction band discontinuities, and we will not repeat that discussion here. As additional core-level to E_v^x binding-energy differences for several semiconductors become available with good precision, the capability of XPS and other photoelectron spectroscopies to monitor interface potential could find wide applications.

ACKNOWLEDGMENT

This research was supported in part by the U.S. Office of Naval Research Contract No. N00014-76-C-1109.

[1]K. Siegbahn, C. Nordling, A. Fahlman, R. Nordberg, K. Hamrin, J. Hedman, G. Johansson, T. Bergmark, S.-E. Karlsson, I. Lindgren, and B. Lindberg, in ESCA-Atomic, Molecular, and Solid State Structure Studied by Means of Electron Spectroscopy Uppsala, 1967 [Nov. Acta R. Soc. Sci. Ups. Ser. IV. 20 (1967)].

[2]J. Auleytner and O. Hornfeldt, Ark. Fys. 23, 165 (1963).

[3]E. A. Kraut, R. W. Grant, J. R. Waldrop, and S. P. Kowalczyk, Phys. Rev. Lett. 44, 1620 (1980).

[4]C. C. Chang, P. H. Citrin, and B. Schwartz, J. Vac. Sci. Technol. 14, 943 (1977).

[5]L. Ley, R. A. Pollak, F. R. McFeely, S. P. Kowalczyk, and D. A. Shirley, Phys. Rev. B 9, 600 (1974).

[6]M. Cardona, C. M. Penchina, N. J. Shevchik, and J. Tejeda, Solid State Commun. 11, 1655 (1972).

[7]D. E. Eastman and J. L. Freeouf, Phys. Rev. Lett. 33, 1601 (1974).

[8]H. Gant and W. Mönch, Surf. Sci. 105, 217 (1981).

[9]B. Z. Olshanetsky, S. M. Repinsky, and A. A. Shklyaev, Surf. Sci. 64, 224 (1977).

[10]D. Haneman, Adv. Phys. 31, 165 (1982).

[11]R. W. Grant, J. R. Waldrop, and E. A. Kraut, Phys. Rev. Lett. 40, 656 (1978).

[12]R. W. Grant, J. R. Waldrop, and E. A. Kraut, J. Vac. Sci, Technol. 15, 1451 (1978).

[13]See, e.g., V. G. Aleshin and Yu. N. Kucherenko, J. Electron Spectrosc. 9, 1 (1976).

[14]U. Gelius, in *Electron Spectroscopy,* edited by D. A. Shirley (North-Holland, Amsterdam, 1972), p. 311.

[15]S. Y. Tong, A. R. Lubinsky, B. J. Mrstik, and M. A. Van Hove, Phys. Rev. B 17, 3303 (1978).

[16]A. Kahn, E. So, P. Mark, and C. B. Duke, J. Vac. Sci. Technol. 15, 580 (1978).

[17]P. Skeath, W. A. Saperstein, P. Pianetta, I. Lindau, and W. E. Spicer, J. Vac. Sci. Technol. 15, 1219 (1978).

[18]D. E. Eastman, T.-C. Chiang, P. Heimann, and F. J. Himpsel, Phys. Rev. Lett. 45, 656 (1980).

[19]D. J. Chadi, Phys. Rev. B 18, 1800 (1978).

[20]D. J. Chadi, J. Vac. Sci. Technol. 15, 1244 (1978).

[21]J. R. Chelikowsky and M. L. Cohen, Solid State Commun. 29, 267 (1979).

[22]T. Murotani, K. Fujiwara, and M. Nishijima, Phys. Rev. B 12, 2424 (1975).

[23]R. Ludeke and A. Koma, Phys. Rev. B 13, 739 (1976).

[24]F. Jona, IBM J. Res. Dev. 9, 375 (1965).

[25]D. Haneman, in *Surface Physics of Phosphors and Semiconductors,* edited by C. G. Scott and C. F. Reed (Academic, London, 1975), p. 1.

[26]D. E. Eastman, W. D. Grobman, J. L. Freeouf, and M. Erbudak, Phys. Rev. B 9, 3473 (1974).

[27]R. Ludeke, L. Ley, and K. Ploog, Solid State Commun. 28, 57 (1978).

[28]D. A. Shirley, Phys. Rev. B 5, 4709 (1972).

[29]G. Aeppli, D. E. Eastman, R. W. Johnson, R. A. Pollak, and H. J. Stolz, J. Electron Spectrosc. 14, 121 (1978).

[30]J. R. Chelikowsky and M. L. Cohen, Phys. Rev. B 14, 556 (1976).

[31]E. A. Kraut, Rev. Geophys. 1, 401 (1963).

[32]V. V. Nemoshkalenko, V. G. Aleshin, and Yu. N. Kucherenko, J. Electron Spectrosc. 13, 361 (1978).

[33]V. V. Nemoshkalenko, V. G. Aleshin, and Yu. N. Kuchesenko, Solid State Commun. 20, 1155 (1976).

[34]T. Jarlborg and A. J. Freeman, Phys. Lett. 74A, 349 (1979).

[35]R. G. Cavell, S. P. Kowalczyk, L. Ley, R. A. Pollak, B. Mills, D. A. Shirley, and W. Perry, Phys. Rev. B 7, 5313 (1973).

[36]P. H. Citrin, G. K. Wertheim, and Y. Baer, Phys. Rev. Lett. 41, 1425 (1978).

[37]G. K. Wertheim, M. A. Butler, K. W. West, and D. N. E. Buchanan, Rev. Sci. Instrum. 45, 1369 (1974).

[38]P. H. Citrin, G. K. Wertheim, and Y. Baer, Phys. Rev. B 16, 4256 (1977).

[39]D. W. Marquardt, J. Soc. Indust. Appl. Math. 11, 431 (1963).

[40]R. L. Kelly *et al.*, Rev. Mod. Phys. 52, S36 (1980).

[41]J. A. Knapp and G. J. Lapeyre, J. Vac. Sci. Technol. 13, 757

(1976).
[42]R. Ludeke and L. Ley, *Proceedings of the 14th International Conference on the Physics of Semiconductors, Edinburgh, 1978,* edited by B. L. H. Wilson (IOP, Bristol, 1978), Chap. 28, p. 1069.
[43]A. Zunger, Phys. Rev. B 22, 959 (1980).
[44]G. P. Williams, R. J. Smith, and G. J. Lapeyre, J. Vac. Sci. Technol. 15, 1249 (1978).
[45]A. Huijser, J. van Laar, and T. L. van Rooy, Phys. Lett. 65A, 337 (1978).
[46]K. C. Pandey and J. C. Phillips, Phys. Rev. Lett. 32, 1433 (1974).
[47]S. Brennan, J. Stöhr, R. Jaeger, and J. E. Rowe, Phys. Rev. Lett. 45, 1414 (1980).
[48]F. H. Himpsel, D. E. Eastman, P. Heimann, B. Reihl, C. W. White, and D. M. Zehner, Phys. Rev. B 24, 1120 (1981).
[49]F. J. Himpsel, P. Heimann, T.-C. Chiang, and D. E. Eastman, Phys. Rev. Lett. 45, 1112 (1980).
[50]D. Chadwick and M. A. Karolewski, J. Electron Spectrosc. 24, 181 (1981).
[51]J. Szajman, J. G. Jenkin, J. Liesegang, and R. C. G. Leckey, J. Electron Spectrosc. 14, 41 (1978).
[52]R. W. Grant, J. R. Waldrop, S. P. Kowalcyzk, and E. A. Kraut, J. Vac. Sci. Technol. 19, 477 (1981).
[53]W. E. Spicer, I. Lindau, P. Skeath, and C. Y. Su, J. Vac. Sci. Technol. 17, 1019 (1980).
[54]J. Chelikowsky, D. J. Chadi, and M. L. Cohen, Phys. Rev. B 8, 2786 (1973).
[55]F. Herman, C. D. Kuglin, K. F. Cuff, and R. L. Kortum, Phys. Rev. Lett. 11, 541 (1963).